Single-Cell Memory Regulates a Neural Circuit for Sensory Behavior

Kobayashi, Kyogo
Division of Biological Science, Graduate School of Science, Nagoya University

Nakano, Shunji
Division of Biological Science, Graduate School of Science, Nagoya University

Amano, Mutsuki
Department of Cell Pharmacology, Graduate School of Medicine, Nagoya University

Tsuboi, Daisuke
Department of Cell Pharmacology, Graduate School of Medicine, Nagoya University

他

出版情報：Cell Reports. 14 (1), pp.11-21, 2016-01-05. Elsevier
バージョン：

Report

Cell Reports

Single-Cell Memory Regulates a Neural Circuit for Sensory Behavior

Graphical Abstract

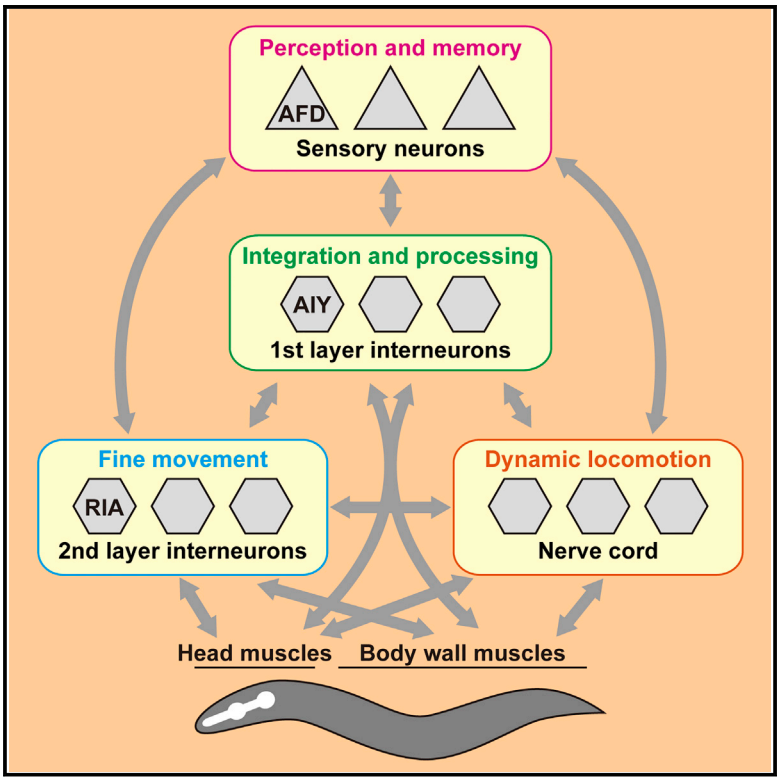

Highlights

- A single thermosensory neuron is capable of memorizing a temperature
- This single-cell memory shows variability between individuals
- The CaMKI/IV and Raf pathway modulates variability in single-cell memory
- The variability of the single-cell memory underlies premotor neuron activity

Authors

Kyogo Kobayashi, Shunji Nakano, Mutsuki Amano, ..., Genta Yokoyama, Kozo Kaibuchi, Ikue Mori

Correspondence

m46920a@nucc.cc.nagoya-u.ac.jp

In Brief

Kobayashi et al. show that a single sensory neuron can memorize information without any neural connections and suggest that single-cell memory can underlie differences between individual responses.

Kobayashi et al., 2016, Cell Reports *14*, 1–11
January 5, 2016
http://dx.doi.org/10.1016/j.celrep.2015.11.064

CellPress

Please cite this article in press as: Kobayashi et al., Single-Cell Memory Regulates a Neural Circuit for Sensory Behavior, Cell Reports (2016), http://dx.doi.org/10.1016/j.celrep.2015.11.064

Cell Reports
Report

Single-Cell Memory Regulates a Neural Circuit for Sensory Behavior

Kyogo Kobayashi,[1] Shunji Nakano,[1] Mutsuki Amano,[2] Daisuke Tsuboi,[2] Tomoki Nishioka,[2] Shingo Ikeda,[1] Genta Yokoyama,[1] Kozo Kaibuchi,[2] and Ikue Mori[1,3,*]
[1]Division of Biological Science, Graduate School of Science, Nagoya University, Nagoya 464-8602, Japan
[2]Department of Cell Pharmacology, Graduate School of Medicine, Nagoya University, Nagoya 466-8550, Japan
[3]CREST, JST, 4-1-8 Honcho, Kawaguchi, Saitama, 332-0012, Japan
*Correspondence: m46920a@nucc.cc.nagoya-u.ac.jp
http://dx.doi.org/10.1016/j.celrep.2015.11.064

SUMMARY

Unveiling the molecular and cellular mechanisms underlying memory has been a challenge for the past few decades. Although synaptic plasticity is proven to be essential for memory formation, the significance of "single-cell memory" still remains elusive. Here, we exploited a primary culture system for the analysis of *C. elegans* neurons and show that a single thermosensory neuron has an ability to form, retain, and reset a temperature memory. Genetic and proteomic analyses found that the expression of the single-cell memory exhibits inter-individual variability, which is controlled by the evolutionarily conserved CaMKI/IV and Raf pathway. The variable responses of a sensory neuron influenced the neural activity of downstream interneurons, suggesting that modulation of the sensory neurons ultimately determines the behavioral output in *C. elegans*. Our results provide proof of single-cell memory and suggest that the individual differences in neural responses at the single-cell level can confer individuality.

INTRODUCTION

Whether a single cell can store information of past experience is a long-lasting question in neuroscience. While a large number of studies have shown that memory is established by an ensemble of neurons, recent studies have also suggested that synapse-independent cellular mechanisms of individual cells are also important for information storage (Sidiropoulou et al., 2009; Zhang and Linden, 2003). However, whether a memory is formed and stored within a single cell still remains elusive.

To ask whether a single cell can form and store memory on its own, we dissected the nervous system of the nematode *C. elegans*. *C. elegans* can remember a variety of environmental cues such as taste, smell, and temperature and change its behavioral response based on the memorized information (Sasakura and Mori, 2013). Of these behaviors, thermotaxis involves memorization of the past cultivation temperature. After cultivation at a certain temperature with food, *C. elegans* animals migrate toward the cultivation temperature on a thermal gradient: if animals cultivated at 17°C, 20°C, or 23°C are placed on the thermal gradient, they migrate toward 17°C, 20°C, or 23°C regions, respectively (Hedgecock and Russell, 1975; Jurado et al., 2010).

We previously identified a neural circuit required for thermotaxis. In this circuit, temperature is mainly sensed by a single pair of bilaterally symmetric thermosensory AFD neurons. Subsequently, two pairs of AIY and AIZ interneurons relay the thermal information from AFD to a pair of downstream premotor RIA neurons to generate thermotactic motor outputs (Figure 1A) (Kuhara et al., 2008; Mori and Ohshima, 1995).

Intriguingly, previous studies suggested that the thermosensory AFD neuron can memorize the cultivation temperature. In response to temperature warming, the intracellular calcium concentration of the AFD neuron increases around the cultivation temperature, and the temperature at which calcium increases in AFD can be varied depending on the cultivation temperature (Kimura et al., 2004). Moreover, the temperature-evoked calcium increment of AFD was not affected by mutations that disrupt either one of the pre-synaptic or one of the post-synaptic neurons of AFD (Clark et al., 2006). This observation raised the hypothesis that AFD is capable of not only sensing but also memorizing the temperature. However, the direct proof for the single-cell memory in which temperature memory is initially formed within AFD has been lacking, because the possibility that a cell (or cells) other than AFD transmits the memory information to AFD has still remained (Figure 1B).

In this study, we investigated a memory mechanism within a single cell by exploiting a primary culture system and found that the thermosensory AFD neuron has an ability to acquire, retain, and reset the information of cultivation temperature without any inputs from other cells. Furthermore, this single-cell memory mechanism has a certain level of inter-individual variability, even when the animals were genetically homogeneous and subjected to identical environmental exposure. This difference in single-cell memory between individuals is regulated by CaMKI/IV and its target pathway Raf-MEK-ERK-MED23. Our results provide proof of single-cell memory that exhibits inter-individual variability and suggest that the individual differences in neural responses at the single-cell level can confer individuality by altering complex brain function.

Please cite this article in press as: Kobayashi et al., Single-Cell Memory Regulates a Neural Circuit for Sensory Behavior, Cell Reports (2016), http://dx.doi.org/10.1016/j.celrep.2015.11.064

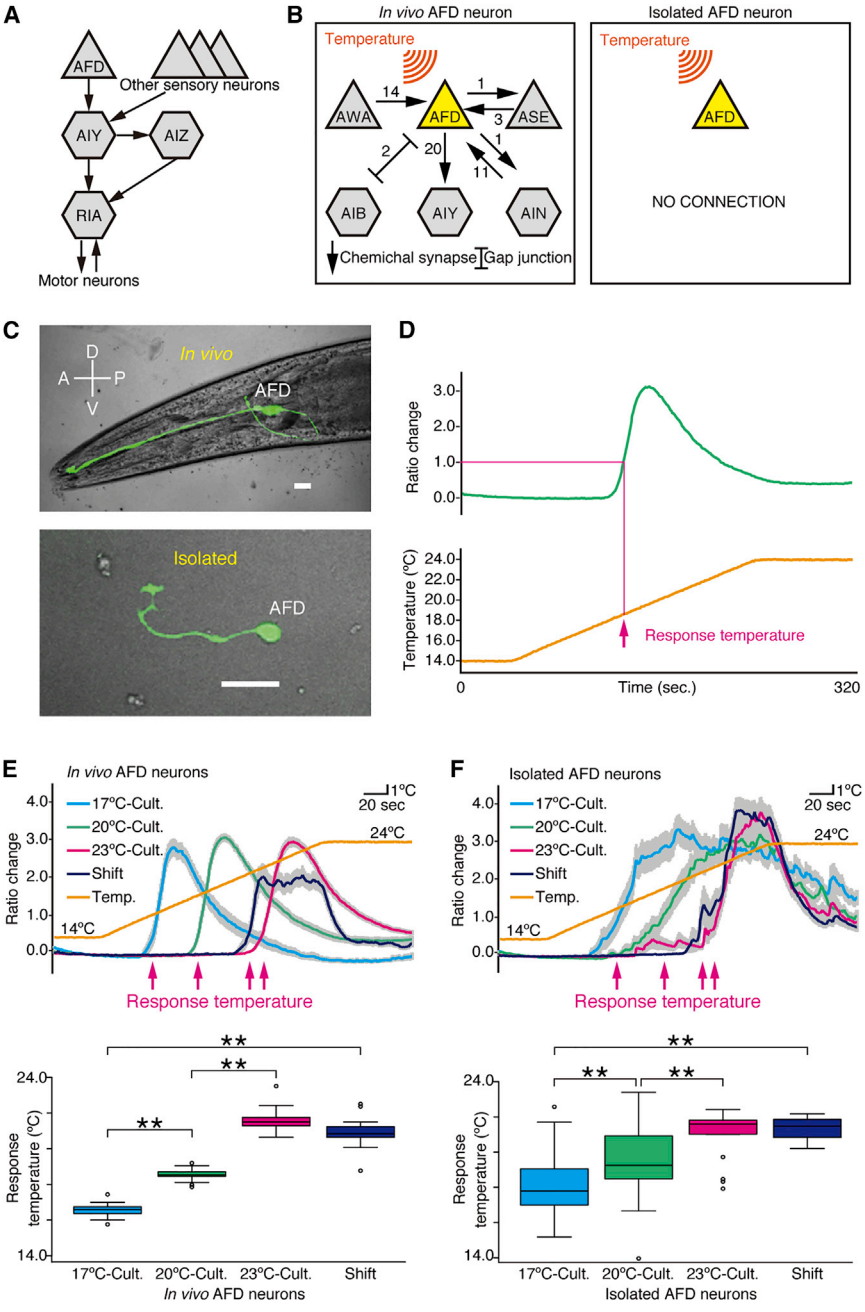

Figure 1. AFD Neuron Cell-Autonomously Remembers the Cultivation Temperature without Any Neural Connections

(A) A proposed thermotaxis neural circuit. The arrows represent synaptic inputs.

(B) In vivo AFD neuron forms synapses with its synaptic partners (left), and isolated AFD neuron has no neural connections (right). Triangles indicate sensory neurons, and hexagons indicate interneurons. The numbers represent the number of synapses.

(C) Expression of *ttx-1p::GFP* in a live animal (top) or a cultured cell (bottom). Scale bars, 20 μm (top) and 10 μm (bottom), respectively. D, dorsal; V, ventral; A, anterior; P, posterior.

(D) Response temperature is defined as the temperature at which GCaMP3/TagRFP fluorescence ratio change first exceeded 1.0 in single-trial calcium imaging and 0.5 in multiple-trial calcium imaging, respectively.

(E and F) Calcium imaging of in vivo AFD cultivated (Cult.) at 17°C (n = 28), 20°C (n = 58), 23°C (n = 46), or shifted from 17°C to 23°C (n = 17) (E) and isolated AFD neurons cultured at 17°C (n = 30), 20°C (n = 38), 23°C (n = 22), or shifted from 17°C to 23°C (n = 16) (F). In boxplots, center lines indicate the medians, box limits indicate the 25th and 75th percentiles as determined by R software, whiskers indicate 1.5 times the interquartile range from the 25th and 75th percentiles, and outliers are represented by dots. Mean ± SEM of ratio change (top) and boxplots of response temperatures (bottom). The red arrows indicate the mean values of the response temperatures. *p < 0.05; **p < 0.01.

See also Figure S1.

RESULTS

A Thermosensory Neuron AFD Harbors Memory Function

To assess whether the thermosensory neuron AFD can memorize the temperature without any inputs from other cells, we obtained primary cultures of AFD neurons and analyzed their memory function in an isolated state (Figure 1B). We adopted a cell-culture method that utilized embryonic cells, aiming to dissociate cells before they form neural connections (Christensen et al., 2002). Briefly, embryonic cells were dissociated from each other and spread at a low cell density (~9 × 10^4 cells per square centimeter) to prevent cell-cell interactions. Culture medium was frequently exchanged (every day and right before calcium imaging) to remove potentially existing secreted molecules. After culturing these isolated cells for several days, we identified mature AFD neurons based on the expression of *ttx-1* promoter-fused GFP, an AFD cell-fate reporter (Satterlee et al., 2001), and confirmed that the cultured AFD was completely isolated without any cell connections (Figure 1C).

We also developed a calcium-imaging system for primary culture of AFD neurons. Calcium dynamics of cultured AFD neurons were then compared with that of in vivo AFD neurons, using the genetically encoded calcium indicator GCaMP3 (Tian et al., 2009), where TagRFP was coexpressed with GCaMP3 to enable ratiometric imaging. We quantified fluorescence signals from AFD soma (Figure S1A) and defined "response temperature" as the temperature at which GCaMP3/TagRFP fluorescence ratio change first exceeded 1.0 (Figure 1D).

We then examined temperature-evoked calcium dynamics in cultured AFD neurons and found that, similar to the responses of in vivo AFD neurons (Figure 1E), calcium level in isolated AFD neurons increased in response to warming, and their response temperatures were in a distinct range depending on the previous culture temperatures (Figure 1F). To investigate whether these responses of cultured AFD neurons resulted from a general intrinsic property of the cultured neurons or from the thermosensory function of AFD, we analyzed calcium responses in chemosensory neurons and mutant AFD neurons. AWB olfactory and ASER gustatory neurons, both of which are classified as amphid sensory neurons like AFD, showed no calcium response to thermal stimuli in either cultured states or in vivo states (Figure S1B; Table S1). In addition, mutations in the molecular components essential for AFD thermosensation, GCY-8, GCY-18, and GCY-23 guanylyl cyclases, or the TAX-4 cGMP-gated cation channel (Inada et al., 2006; Komatsu et al., 1996), abolished thermal response of AFD in both cultured and in vivo conditions (Figure S1B; Table S1). These results suggest that AFD can memorize temperature without any inputs from other cells and that the memory-based calcium response requires the thermosensory machinery in AFD.

To address whether isolated AFD can reset the temperature memory, we next subjected isolated AFD neurons to a temperature shift from 17°C to 23°C and found that isolated AFD neurons changed their response temperatures to the new culture temperature: the response temperature more than 6 hr after the temperature shift was comparable to that of AFD neurons continuously cultured at 23°C (Figures 1E and 1F). These results demonstrate that the AFD neuron itself has the ability to form, retain, and reset the temperature memory.

AFD Neuron Exhibits Variability in Single-Cell Memory between Individuals

Through the analysis of temperature memory in AFD, we found that AFD neurons had a certain range of variability in response temperature. Upon a linear temperature warming, AFD neurons of 20°C-cultivated animals showed calcium responses within a temperature range of about 17.7°C to 19.2°C (Figure 2A). This variability in response temperature was observed at all cultivation temperatures tested (Figures 2A and S2A) and was most evident when AFD neurons of 23°C-cultivated animals were subjected to stepwise temperature warming (Figure 2B).

Next, we subjected a single AFD neuron to repeated trials of calcium imaging to assess whether this variable response of AFD results from animal-to-animal variability or trial-to-trial variability. AFD neurons of 23°C-cultivated animals were subjected to six trials of calcium imaging and showed that their response temperatures were almost invariable within the same animal but variable among different animals: trial-to-trial variability, the average value of differences between two response temperatures observed by two consecutive trials in the same animal, was about 0.4°C, whereas animal-to-animal variability, the average value of differences between the maximum and minimum of the response temperatures observed in the jth trial (j = 1–6) of all animals examined, was about 1.4°C (Figures 2C and 2D; see Supplemental Experimental Procedures for calculations of these values). These results suggest that AFD neuron had animal-to-animal variability in thermal response.

Next, we investigated whether the variability in AFD thermal response is an intrinsic property of AFD. Similar to the responses of in vivo AFD neurons, the calcium level in isolated AFD neurons increased depending on the previous culture temperature, and the response temperatures were distributed within a certain range (Figure 2A). To assess whether the variable response of cultured AFD results from the cell-to-cell variability or the trial-to-trial variability, we subjected cultured AFD neurons to repeated trials of calcium imaging. The 23°C-cultured isolated AFD neurons were subjected to six trials of calcium imaging, and, similar to in vivo conditions, inter-individual variability in response temperature was larger than trial-to-trial variability (Figure 2D). Thus, these results suggest that the AFD neuron cell-autonomously memorizes the cultivation temperature and that the cell-to-cell variability in temperature memory is an intrinsic property of the AFD neuron.

CaMKI/IV Acts to Suppress the Inter-individual Variability of Temperature Memory in AFD

To date, cAMP response element binding protein (CREB) and calcium-calmodulin-dependent protein kinase II (CaMKII) are well-known key molecules that establish memory (Kandel et al., 2014; Lisman et al., 2002). However, neither *crh-1* mutants that lacked a *C. elegans* CREB homolog (Nishida et al., 2011) nor *unc-43* mutants that lacked the *C. elegans* CaMKII ortholog (Reiner et al., 1999) showed a severe defect in the variable calcium response of AFD (Figure S2B). These results suggest that CRH-1/CREB and UNC-43/CaMKII are not crucial for the variability of temperature memory in AFD. To identify the molecular determinant for the variability of AFD temperature memory, we focused next on the gene *cmk-1*, which encodes the predicted *C. elegans* ortholog of mammalian CaMKI and CaMKIV (Eto et al., 1999). A recent study on CMK-1 reported that the averaged value of the AFD response temperature was abnormally low in *cmk-1* mutants (Yu et al., 2014).

Then, we examined whether this low response temperature is either due to high variability of individual response temperatures with a large fraction of the responses with low response temperatures or due to lower response temperatures exhibited by the population as a whole without changing the variability of individual responses. We subjected AFD neurons of 23°C-cultivated *cmk-1* mutants to six trials of calcium imaging and compared the variability to that of wild-type animals. While trial-to-trial variability in wild-type and *cmk-1* animals were comparable, animal-to-animal variability in *cmk-1* mutants was significantly larger than that of wild-type animals, showing that the lack of CMK-1 increases the animal-to-animal variability of AFD (Figure 2D). We also subjected AFD neurons of *cmk-1* mutants to single-trial calcium imaging and found that response temperatures were abnormally perturbed at both 20°C and 23°C cultivation (Figures 2E and 2F; Figure S2C). While wild-type AFD neurons of 23°C-cultivated animals initiated calcium responses within a temperature range of about 19.0°C to 22.0°C, *cmk-1* mutant AFD neurons started to respond within a wider temperature range of about 16.0°C to 21.0°C (Figures 2E and 2F). Next, we isolated AFD neurons from *cmk-1* mutants and examined

Please cite this article in press as: Kobayashi et al., Single-Cell Memory Regulates a Neural Circuit for Sensory Behavior, Cell Reports (2016), http://dx.doi.org/10.1016/j.celrep.2015.11.064

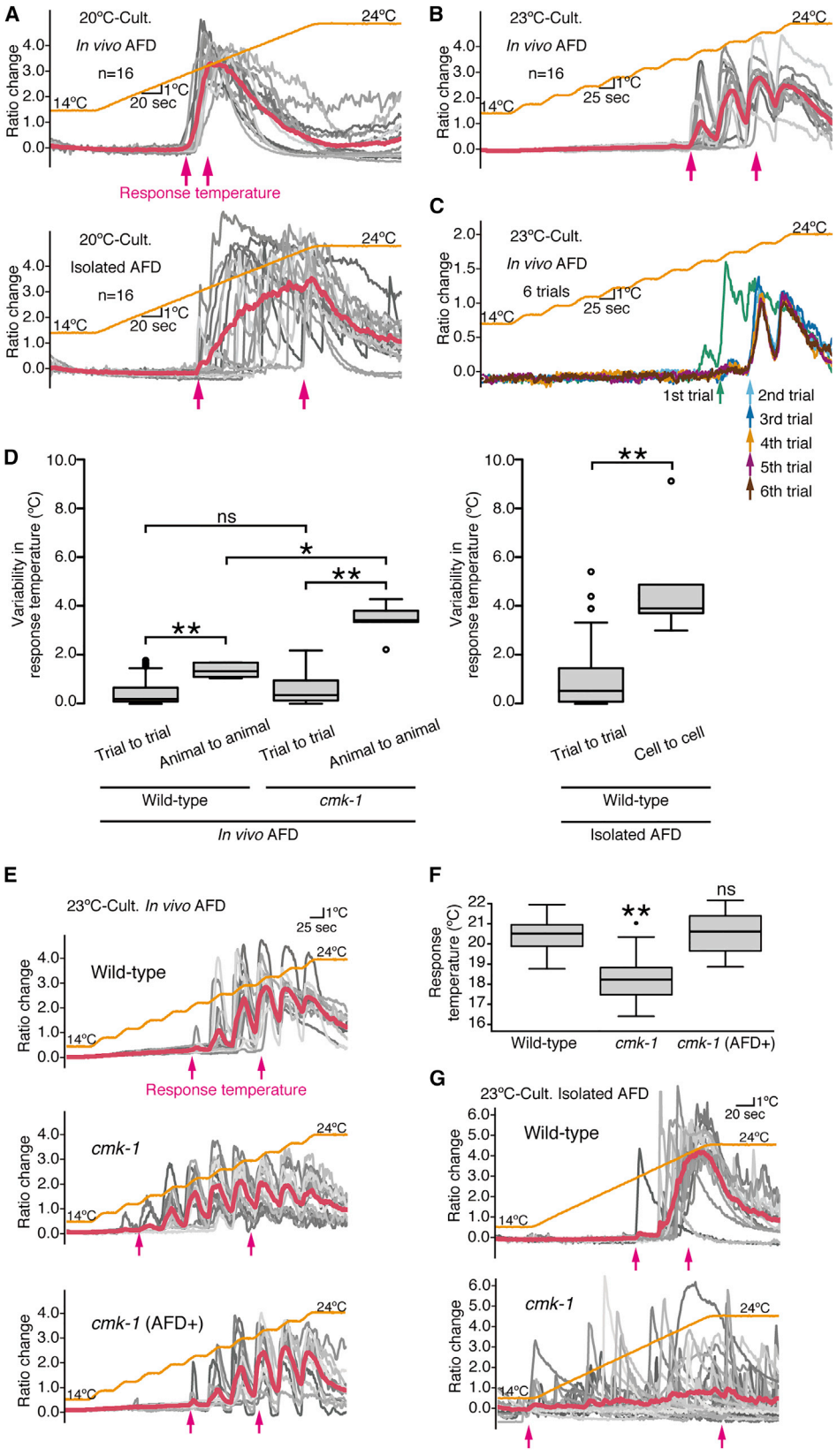

(legend on next page)

response temperature to investigate whether this abnormal variability in *cmk-1* mutants is caused by the lack of CMK-1 in AFD. Similar to in vivo conditions, isolated *cmk-1* mutant AFD neurons also showed increased variability in response temperature, suggesting that the lack of CMK-1 only in AFD is responsible for the abnormal variability in response temperature of AFD (Figure 2G). Indeed, expression of a *cmk-1* cDNA only in AFD completely rescued the response temperatures in *cmk-1* mutants, indicating that CMK-1 cell-autonomously acts in AFD (Figures 2E, 2F, and S2C). Thus, these results indicate that CMK-1 functions in AFD to suppress the animal-to-animal variability in the temperature memory-based calcium response of AFD.

Identification of a Substrate of CMK-1

Although CaMKI and CaMKIV are highly expressed in the mammalian brain and thought to play important roles, their functions and interacting molecules have been largely unknown (Wayman et al., 2008). To identify the molecular pathway involving CaMKI/IV, we undertook two different types of screens: one was a forward suppressor screen of *cmk-1* mutants to look for genetic interactors of CMK-1. The other was a phosphoproteomic screen to look for biochemical substrates of CMK-1.

In the suppressor screen, we utilized pleiotropic defects of *cmk-1* mutants: *cmk-1* mutants showed abnormally low expression of *nhr-38* promoter-fused GFP, an AFD neuron-specific GFP marker (Satterlee et al., 2004). Therefore, we mutagenized *cmk-1* mutants carrying *nhr-38* promoter-fused GFP and found that a mutation in *sur-2* gene that encodes the ortholog of human MED23, a subunit of transcription mediator complex (Singh and Han, 1995), restored the expression of the GFP marker in a *cmk-1* mutant background (Figures S3A and S3B).

In the phosphoproteomic screen, an in vitro phosphorylation assay and subsequent high-accuracy mass spectrometry revealed a list of *C. elegans* proteins that were phosphorylated by human CaMKI (Figure S3C) (The list of proteins phosphorylated by CaMKI and the detailed information about the phosphorylation sites will be deposited in the Kinase-Associated Neural Phospho-Signaling (KANPHOS) database: https://srpbsg01.unit.oist.jp/index.php?ml_lang=en.) Among 38 phosphorylated proteins, we focused on LIN-45, the *C. elegans* ortholog of Raf kinase, since LIN-45 was shown to act upstream of SUR-2 in a signaling pathway that determines the development of the *C. elegans* vulva, in which the growth factor signal is mediated by LIN-45 (Raf), MEK-2 (MEK), MPK-1 (ERK), and SUR-2 (MED23) (Figure 3A) (Han et al., 1993; Singh and Han, 1995). We confirmed that *C. elegans* CMK-1 could also phosphorylate LIN-45 in vitro, verifying that LIN-45 is, indeed, a substrate of CMK-1 (Figure S3D).

The Raf Kinase Pathway Generates the Variability of Temperature Memory of AFD

To assess the involvement of the Raf pathway in temperature memory variability in AFD, we analyzed temperature-evoked calcium dynamics of AFD in the Raf pathway mutants: *lin-45*, *mek-2*, *mpk-1*, and *sur-2*. Surprisingly, mutations in Raf pathway genes reduced the variability of response temperatures of AFD. The wild-type response temperatures distributed within a temperature range of about 19.0°C to 22.0°C. By contrast, the response temperatures of the Raf pathway mutants were within a temperature range of about 20.5°C to 21.5°C (Figures 3B and 3C). This low variability in the response temperatures of Raf pathway mutants seemed opposite to the phenotype of *cmk-1* mutants, which showed larger variability in response temperatures of AFD (Figure 3D). These results suggested that the Raf pathway acts to increase the variability of the single-cell memory mechanism of AFD in contrast to CMK-1 that acts to reduce the variability.

Next, we investigated the genetic interaction between CMK-1 and the respective Raf pathway molecules, LIN-45, MEK-2, MPK-1, and SUR-2. *cmk-1 lin-45* double mutants exhibited almost normal calcium responses, showing that a loss-of-function mutation in *lin-45* suppressed the *cmk-1* abnormality (Figures 3B and 3D). Similarly, a loss-of-function mutation in *mek-2*, *mpk-1*, or *sur-2* also restored the normal response temperatures in a *cmk-1* mutant background (Figure 3D). The expression of a *lin-45* cDNA, specifically in the AFD of *cmk-1 lin-45* double mutants, resulted in a phenotype similar to that of a *cmk-1* single mutant, suggesting that LIN-45 Raf acts cell-autonomously in AFD (Figure 3D). Furthermore, these Raf pathway mutations also suppressed the abnormally low expression of the AFD thermosensory machinery gene *gcy-8* in

Figure 2. AFD Neuron Shows Inter-individual Variability in the Temperature Memory

(A and B) Single-trial calcium imaging of 20°C-cultivated in vivo AFD neurons (A, top) and isolated AFD neurons (A, bottom) subjected to linear temperature warming; and 23°C-cultivated in vivo AFD neurons (B) subjected to stepwise temperature warming. n = 16 for each.

(C) Multiple-trial calcium imaging of in vivo AFD cultivated at 23°C. The orange line indicates temperature. The colored arrows indicate the response temperatures observed at each of the six trials.

(D) Boxplot of trial-to-trial variability and animal-to-animal variability in response temperature. In vivo AFD of wild-type animals (n = 19), *cmk-1* mutants (n = 8), and cultured AFD neurons isolated from wild-type animals (n = 8) were cultivated at 23°C and subjected to six trials of calcium imaging. Stepwise warming and linear warming were applied to in vivo AFD and isolated AFD, respectively.

(E) Calcium imaging of in vivo AFD of wild-type animals (n = 38), *cmk-1* mutants (n = 36), and *cmk-1* mutants expressing a wild-type *cmk-1* cDNA only in AFD (n = 14) cultivated at 23°C.

(F) Boxplot of response temperatures derived from the dataset shown in (E). Steel test was applied to compare the response temperatures in mutants with that in wild-type controls.

(G) Calcium imaging of 23°C-cultured AFD isolated from wild-type animals (n = 18) and *cmk-1* mutants (n = 38).

In (A), (B), (E), and (G), the gray lines indicate individual traces of ratio change, and the red line represents the average of individual ratio changes. The red arrows indicate the lowest and highest response temperatures. In box plots, center lines indicate the medians, box limits indicate the 25th and 75th percentiles as determined by R software, whiskers indicate 1.5 times the interquartile range from the 25th and 75th percentiles, and outliers are represented by dots. *$p < 0.05$; **$p < 0.01$; ns, not significant ($p > 0.05$).

See also Figure S2.

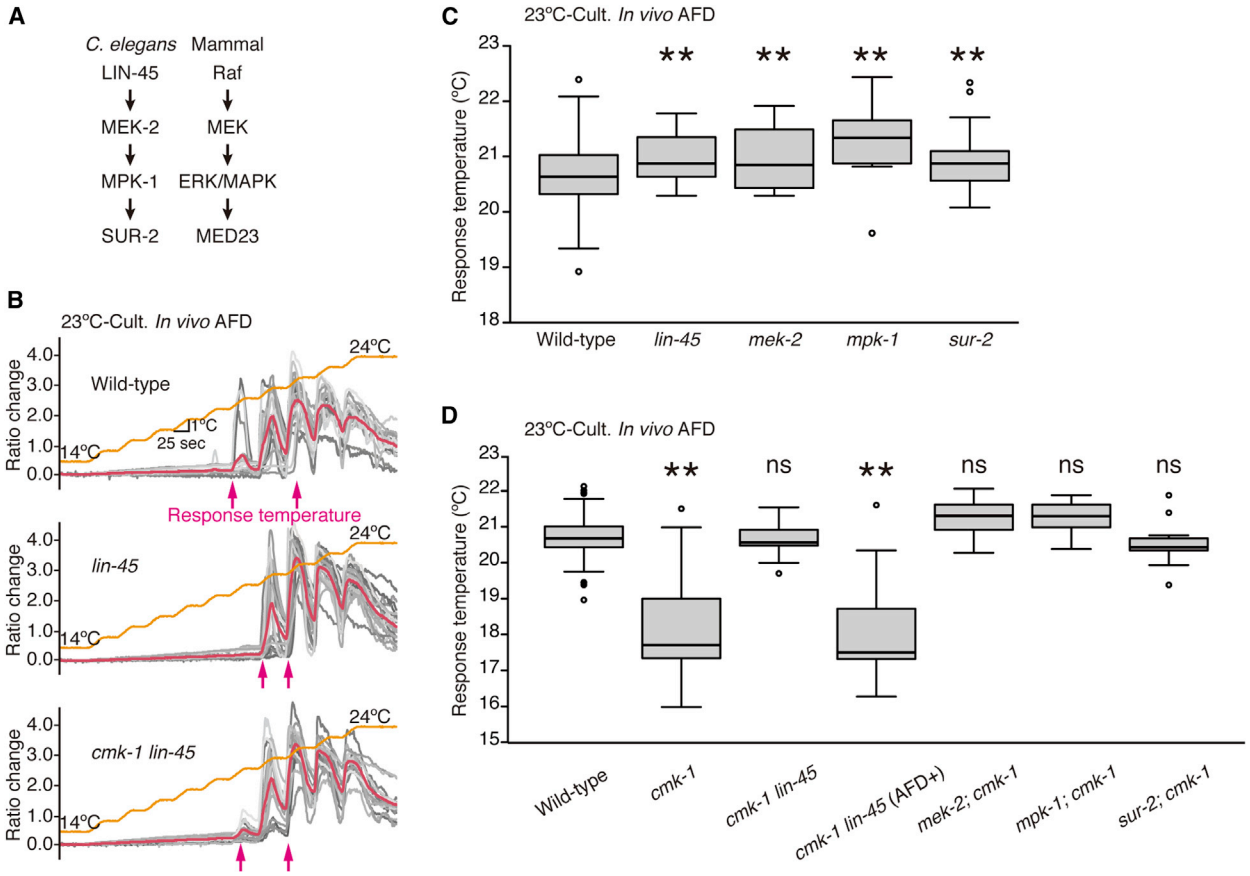

Figure 3. Raf Pathway Regulates the Variability of AFD Memory Representation Downstream of CMK-1

(A) Conserved Raf kinase pathway in *C. elegans* and mammals.

(B) Calcium imaging of AFD in wild-type animals (n = 20), *lin-45* mutants (n = 22), and *cmk-1 lin-45* double mutants (n = 22) cultivated (Cult.) at 23°C. The gray lines indicate individual traces of ratio change, and the red lines represent the average of individual ratio changes. The red arrows indicate the lowest and highest response temperatures.

(C) Boxplot of response temperatures in wild-type animals (n = 48), *lin-45* mutants (n = 38), *mek-2* mutants (n = 16), *mpk-1* mutants (n = 16), and *sur-2* mutants (n = 13) cultivated at 23°C. Steel test was applied to compare the response temperatures in mutants with that in wild-type controls.

(D) Boxplot of response temperatures in wild-type animals (n = 68), *cmk-1* mutants (n = 63), *cmk-1 lin-45* double mutants (n = 37), *cmk-1 lin-45* double mutants expressing the wild-type form of a *lin-45* cDNA only in AFD (n = 33), *mek-2; cmk-1* double mutants (n = 13), *mpk-1; cmk-1* double mutants (n = 14) and *sur-2; cmk-1* double mutants (n = 14) cultivated at 23°C. Steel test was applied to compare the response temperatures in mutants with that in wild-type controls.

*$p < 0.05$; **$p < 0.01$; ns, not significant ($p > 0.05$). In boxplots, center lines indicate the medians, box limits indicate the 25th and 75th percentiles as determined by R software, whiskers indicate 1.5 times the interquartile range from the 25th and 75th percentiles, and outliers are represented by dots.

See also Figures S3 and S4.

cmk-1 mutant background (Supplemental Results; Figure S4). These results suggest that the CaMKI/IV and Raf pathway mediates gene expression of AFD to regulate the response temperature of AFD.

The normal calcium response in *cmk-1 lin-45* double mutants suggested that CMK-1 and LIN-45 are not required for memory formation or subsequent memory retention but for the regulation of variability in memory-based thermal response of AFD after temperature memory is formed and stored within AFD. Therefore, our results are consistent with the possibility that CMK-1 and LIN-45 act to suppress and enhance, respectively, the level of variability in memory-based calcium dynamics of AFD.

Variability in AFD Influences the Variability in the Activity of Downstream Neurons and, Consequently, in Thermotaxis Behavior

Next, we addressed how the CaMKI/IV and Raf pathway-mediated variability of sensory response contributes to the final behavioral output. Since the loss of activity of the Raf pathway molecules causes severe lethality and locomotion defects, we examined the thermotaxis behavior of *cmk-1* mutants. While most of the wild-type animals migrated around the cultivation temperature, *cmk-1* mutants dispersed over a wider range of temperatures (Figures 4A–4C). Expression of a *cmk-1* cDNA only in AFD rescued this *cmk-1* mutant phenotype, while the expression of a kinase-negative form (K52M) of *cmk-1* cDNA

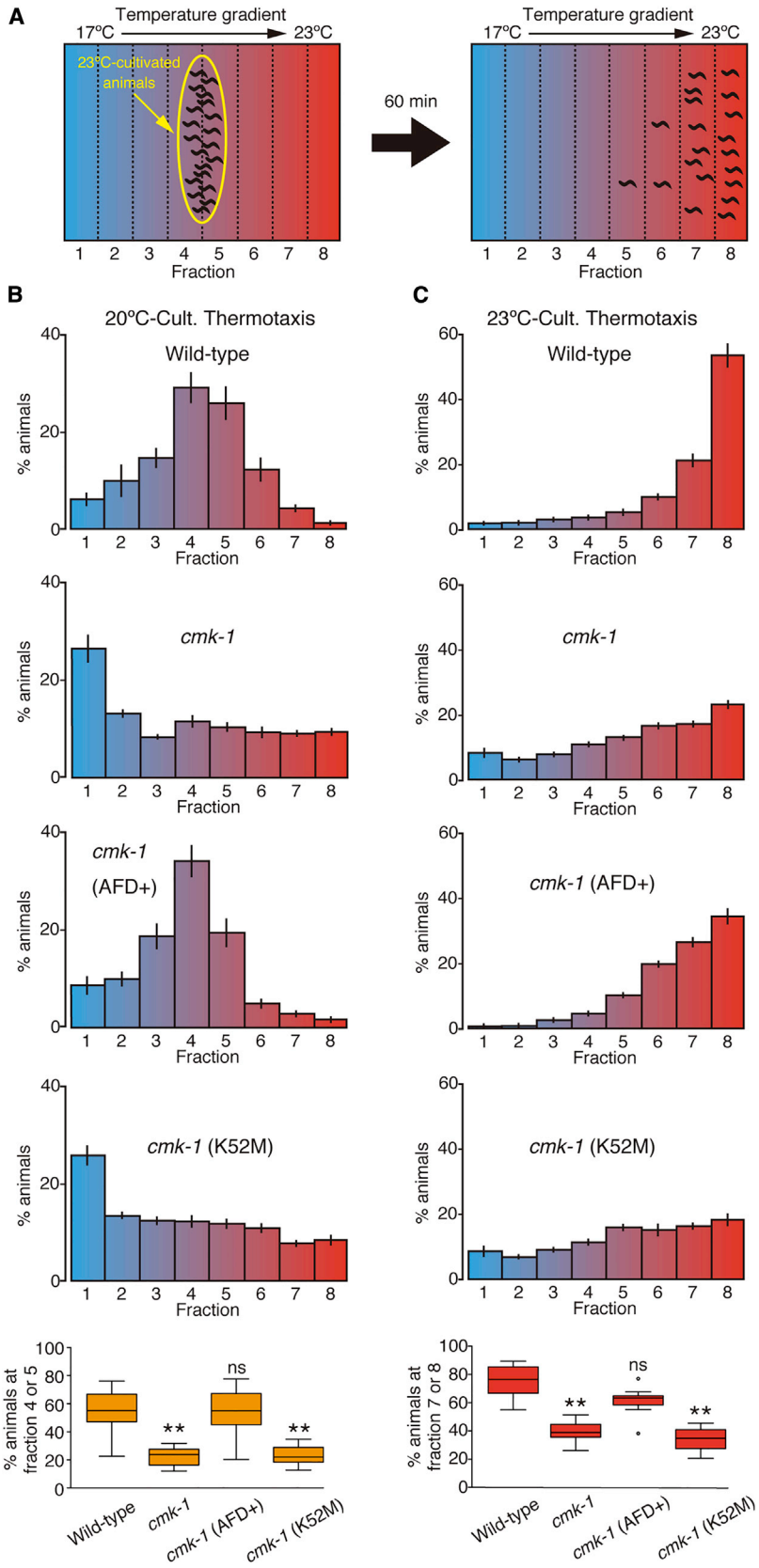

Figure 4. Mutants with High Variability in AFD Response Display Increased Variability in Thermotaxis Behavior

(A) The thermotaxis behavior was tested as previously reported (Ito et al., 2006). Briefly, animals cultivated at a certain temperature were placed at the center of the temperature gradient ranging from 17°C to 23°C. After 60 min, the number of animals in each fraction (1–8) was counted.

(B and C) Thermotaxis behavior of wild-type animals, *cmk-1* mutants, *cmk-1* mutants expressing the wild-type form of a *cmk-1* cDNA only in AFD, and *cmk-1* mutants expressing a kinase-negative form (K52M) of the *cmk-1* cDNA only in AFD cultivated (Cult.) at 20°C (B) or 23°C (C). n = 12 for each. Boxplots represent the percentage of animals that migrated to the cultivation temperature region (fraction 4 or 5 in B and fraction 7 or 8 in C). Steel test was applied to compare the thermotaxis behavior in mutants with that in wild-type controls. In boxplots, center lines indicate the medians, box limits indicate the 25th and 75th percentiles as determined by R software, whiskers indicate 1.5 times the interquartile range from the 25th and 75th percentiles, and outliers are represented by dots.

Error bars indicate SEM. *p < 0.05; **p < 0.01; ns, not significant (p > 0.05).

Please cite this article in press as: Kobayashi et al., Single-Cell Memory Regulates a Neural Circuit for Sensory Behavior, Cell Reports (2016), http://dx.doi.org/10.1016/j.celrep.2015.11.064

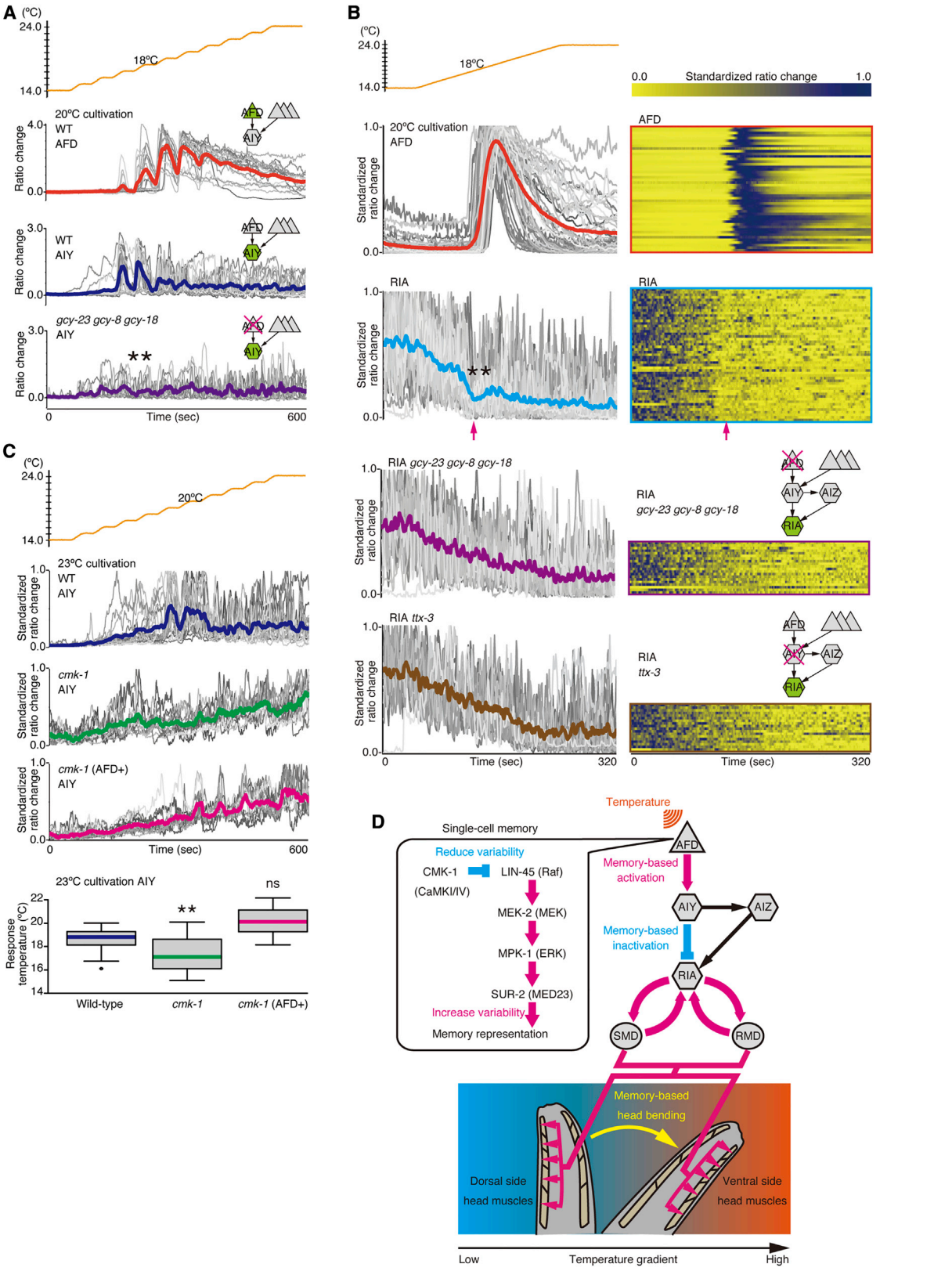

(legend on next page)

failed to rescue the behavioral abnormalities (Figures 4B and 4C). These results suggest that the level of the animal-to-animal variability in the AFD sensory response strongly influences the level of variability in final behavioral output.

To ask how the variability of the temperature perception by AFD affects the activity of downstream neurons to establish thermotaxis, we next analyzed the temperature-evoked calcium dynamics of the AIY interneuron, a major post-synaptic neuron of AFD, and the RIA premotor neuron, a major post-synaptic neuron of AIY (White et al., 1986). We found that AIY exhibits large calcium increments at 2–3°C below the cultivation temperature (Figure 5A) and that the calcium activity of RIA is suppressed at a similar temperature (Figure 5B). In *gcy-23 gcy-8 gcy-18* triple mutants, which are defective in the thermosensory function of AFD (Inada et al., 2006), neither the large calcium increment in AIY nor the suppression of calcium events in RIA was detected, indicating that thermosensation in AFD is required to evoke these downstream neural circuit dynamics (Figures 5A and 5B). In addition, *ttx-3* mutants, which are defective in AIY function (Hobert et al., 1997), did not show the temperature-evoked suppression of RIA activity (Figure 5B). Therefore, these results indicate that the thermal response of AFD evokes the large calcium increments of AIY, which, in turn, suppresses the calcium activity of RIA.

Next, we examined the response temperatures of AIY in *cmk-1* mutants. We found that, similar to the case of AFD, the AIY neuron of *cmk-1* mutants showed abnormally increased variability in response temperatures: while response temperatures of 23°C-cultivated wild-type AIY neurons were within a temperature range of about 16.8°C to 20.0°C, those of *cmk-1* mutant AIY neurons were distributed within a wider temperature range of about 15.3°C to 20.1°C (Figure 5C). Expression of a *cmk-1* cDNA only in AFD rescued these abnormal response temperatures of AIY in *cmk-1* mutants, indicating that the CMK-1-mediated variability of AFD influences the variability of the AIY response (Figure 5C). Therefore, these results indicate that the CaMKI/IV-Raf pathway regulates the variability of temperature perception in AFD and, consequently, the variability of downstream neural circuit dynamics (Figure 5D).

DISCUSSION

In this study, we discovered that the *C. elegans* thermosensory AFD neuron is capable of memorizing a temperature without any inputs from other cells. Integrating the information of present ambient temperature and memorized cultivation temperature, AFD increases intracellular calcium levels at a certain temperature range that nearly corresponds to the cultivation temperature. CaMKI/IV influences the variability and threshold temperature of calcium responses of AFD and, consequently, thermotaxis behavior through the interaction with the Raf-MEK-ERK-MED23 pathway. Slightly below the cultivation temperature, a calcium increment of AFD triggers a large calcium transient of AIY, which, in turn, suppresses the calcium spikes of RIA to generate a memory-based motor output.

Analysis of *C. elegans* Sensory Neurons in Cell Culture System and Single-Cell Memory

More than 100 years ago, Santiago Ramón y Cajal proposed a theory that memory is stored as changes of connectivity between nerve cells (Ramón y Cajal, 1894). Our results demonstrated that memory can also be formed and stored within a single cell by a neural circuit-free mechanism. Notably, a study on mouse brains showed a possibility that a single cell of the prefrontal cortical neurons might be able to store a memory (Sidiropoulou et al., 2009). Our results, together with this observation, suggest that a memory is attributable to a single cell in the nervous system of species ranging from *C. elegans* to mammals and that memory representation in a single cell has a prominent role in behavior.

Here, we exploited a primary cell culture system, in which individual neurons can be extensively analyzed in a "circuit-free" environment, and provided proof for single-cell memory. Indeed, recent studies have demonstrated that sensory neurons in *C. elegans* exhibit a variety of neuronal plasticity (Kunitomo et al., 2013; Sasakura and Mori, 2013). The emerging picture from our present and previous studies is that the sensory system in *C. elegans*, comprising limited numbers of sensory neurons, possesses potentially quite complex brain functions within a sensory neuron. Nevertheless, it is difficult to explicitly assess

Figure 5. Variability in AFD Memory Evokes Variability in Downstream Neural Circuit Dynamics

(A) Calcium imaging of AFD in wild-type animals (n = 17) and AIY in wild-type animals (n = 19) and *gcy-23 gcy-8 gcy-18* triple mutants (n = 11) cultivated at 20°C. The gray lines indicate individual traces of ratio change, and the colored lines represent the average of individual ratio changes. The double asterisk (**) indicates the statistical significance between the maximum values of AIY ratio change of wild-type and *gcy* triple-mutant animals.

(B) Calcium imaging of AFD in wild-type animals (n = 48), RIA in wild-type animals (n = 50), *gcy-23 gcy-8 gcy-18* mutants (n = 20), and *ttx-3* mutants (n = 18) cultivated at 20°C. Since the maximum values of GCaMP3/TagRFP fluorescence ratio change in wild-type RIA neurons were considerably different, we standardized the maximum values of GCaMP3/TagRFP ratio change of RIA as 1.0 to analyze the timing of calcium event. The gray lines indicate individual traces of standardized ratio change, and the colored lines represent the average of individual standardized ratio changes (left). The heatmaps indicate individual traces of standardized ratio change (right). The double asterisk (**) indicates the statistical significance between the values of standardized ratio changes at the 16°C and the 18°C temperature points. The red arrows indicate the 18°C temperature point.

(C) Response temperatures of AIY in wild-type (WT) animals (n = 19), *cmk-1* mutants (n = 12) and *cmk-1* mutants expressing a wild-type *cmk-1* cDNA only in AFD (n = 12) cultivated at 23°C. As in the case of RIA, we standardized the maximum values of ratio change as 1.0 and defined response temperature of AIY as the temperature at which standardized ratio change of AIY first exceeded 0.5 to reliably analyze the timing of calcium events of AIY. The gray lines indicate individual traces of standardized ratio change, and the colored lines represent the average of individual standardized ratio changes. Boxplot represents response temperatures of AIY. Steel test was applied to compare the response temperatures in mutants with that in wild-type controls. In boxplots, center lines indicate the medians, box limits indicate the 25th and 75th percentiles as determined by R software, whiskers indicate 1.5 times the interquartile range from the 25th and 75th percentiles, and outliers are represented by dots.

(D) Schematic of the *C. elegans* memory circuitry.

Please cite this article in press as: Kobayashi et al., Single-Cell Memory Regulates a Neural Circuit for Sensory Behavior, Cell Reports (2016), http://dx.doi.org/10.1016/j.celrep.2015.11.064

whether the plasticity resides in a sensory neuron itself or a neuron-to-neuron connectivity. Hence, we suggest that the primary cell culture system can shed light into this problem and provide a new avenue for the analysis of sensory neurons in *C. elegans*.

Single-Cell-Memory-Driven Neural Circuit Dynamics Generate Memory-Based Motor Output

We revealed that the Raf kinase pathway, Raf-MEK-ERK-MED23, promotes inter-individual variability of single-cell memory. In the thermotaxis neural circuit, the variability of AFD activity regulated by the CaMKI/IV-Raf pathway affects the response temperature of AIY, and AIY suppresses the calcium transients of RIA. RIA densely connects to head motor neurons (White et al., 1986), and *C. elegans* changes its locomotory direction by changing the head direction when crawling forward on a solid surface. Thus, our results suggest that the calcium increment of AFD and subsequent downstream neural circuit dynamics elicit a crucial head movement, such as a directional change of the head toward the memorized temperature. The distinct response properties of individual AFD neurons might thus generate variability in aspects of the head movement and result in differences in behavior between the individuals of a population. On a thermal gradient, AFD neurons of individual animals respond to a temperature environment with slightly different calcium dynamics, and variability in these AFD calcium dynamics might induce the individual differences in the dynamics of the downstream circuits and, ultimately in the behavior (Figure 5D).

Inter-individual Variability in the Nervous System

Individual differences in functions of the nervous system is the neurobiological basis of individuality, and abnormality in the neural variability is hypothesized to cause human neuropathological diseases such as autism, attention-deficit/hyperactivity disorder, and schizophrenia (Dinstein et al., 2015). Therefore, the regulatory mechanism that controls the magnitude of the variability in the nervous system is crucial for its functions, such as cognition, decision making, and behavior. Given that dysfunction of MED23 was previously reported to be linked to a human intellectual disability (Hashimoto et al., 2011), our results suggest that MED23 contributes to the high-order brain functions through the regulation of neural variability. In conclusion, our findings elucidate that the CaMKI/IV-Raf pathway regulates individual differences in single-cell memory and highlights the evolutionarily conserved molecular pathway as a crucial intrinsic factor that confers individuality in brain function.

EXPERIMENTAL PROCEDURES

Strains

C. elegans were cultivated under standard conditions (Brenner, 1974). Strains used in this study are listed in Table S2.

Primary Cell Culture

Preparation of *C. elegans* primary cell cultures was performed essentially as described previously (Christensen et al., 2002). We isolated eggs from gravid animals and spread dissociated embryonic cells at a low cell density (~9×10^4 cells per square centimeter) onto a coverglass. See also the Supplemental Experimental Procedures.

Calcium Imaging

For in vivo calcium imaging, a single adult animal was placed on a 10% agar pad on a microscope coverslip with 0.4 μl of 0.1 μm polystyrene beads (Polysciences) and covered by a coverslip to immobilize the animals (Kim et al., 2013). For isolated cells, a cell-plated coverslip was placed in a square hole filled with extracellular solution (145 mM NaCl, 5 mM KCl, 5 mM $MgCl_2$, 1 mM $CaCl_2$, 10 mM HEPES, 10 mM D-glucose, pH adjusted with NaOH to 7.2 and osmolality adjusted with sucrose to 340 mOsm). We defined "response temperature" as the temperature at which the GCaMP3/TagRFP fluorescence ratio change first exceeded 1.0 in single-trial calcium imaging. In multiple-trial calcium imaging, weak excitation lights for GCaMP3 or TagRFP fluorescence imaging were used to minimize the effects of long-time exposure to excitation light, such as photobleaching or cell damaging. Due to the difference in excitation energy, the value of GCaMP3/TagRFP fluorescence ratio change was almost half of that in single-trial calcium imaging (Figures 2B and 2C); hence, we defined "response temperature" as a temperature at which GCaMP3/TagRFP fluorescence ratio change first exceeded 0.5 in multiple-trial calcium imaging experiments. See also the Supplemental Experimental Procedures.

Statistics

In boxplots, center lines indicate the medians, box limits indicate the 25th and 75th percentiles as determined by R software, whiskers indicate 1.5 times the interquartile range from the 25th and 75th percentiles, and outliers are represented by dots. For comparison tests, Steel methods or Steel-Dwass methods were applied. Outliers displayed in the boxplot were not removed from statistical tests. In all figures, $^*p < 0.05$, $^{**}p < 0.01$, and $p > 0.05$ is considered as not significant (ns). In comparing the response temperature, samples that showed no or slight GCaMP3/TagRFP fluorescence ratio change (<1.0 in single-trial and <0.5 in multiple-trial calcium imaging experiments) were excluded. The total number of samples recorded and the number of samples that exceeded a 1.0 GCaMP3/TagRFP ratio change are shown in Table S1.

SUPPLEMENTAL INFORMATION

Supplemental Information includes Supplemental Experimental Procedures, Supplemental Results, four figures, and two tables and can be found with this article online at http://dx.doi.org/10.1016/j.celrep.2015.11.064.

AUTHOR CONTRIBUTIONS

K. Kobayashi, S.N., and I.M. designed and interpreted experiments and wrote the paper. K. Kobayashi contributed to all experiments and analyzed data. S.I. and G.Y. conducted calcium imaging in RIA neurons. S.N., M.A., D.T., T.N., and K. Kaibuchi carried out the proteomic screen and analyzed data. M.A. performed the phosphorylation assay.

ACKNOWLEDGMENTS

We thank C. Bargmann for the GCaMP3 construct and the *str-1* promoter; Y. Iino for the *gcy-5* promoter; P. Sengupta for the *cmk-1* cDNA; A. Fire for pPD plasmids; J. McGhee for the *ges-1* promoter; T. Ishihara for the *H13 (nhr-38)* promoter; K. Suzuki for sharing unpublished strains; and T. Jiang for sharing unpublished results; Some strains were provided by the Caenorhabditis Genetic Center (CGC), which is funded by the NIH Office of Research Infrastructure Programs (P40 OD010440). We thank C. Yokoyama for critical advice; A. Giles and P. Jurado for helpful comments; and members of the I.M. laboratory for helpful discussion. K. Kobayashi was a Research Fellow of the Japan Society for the Promotion of Science (JSPS). I.M. is a Scholar of the Institute for Advanced Research in Nagoya University. This work was supported by a Grant-in-Aid for JSPS Fellows; a Grant-in-Aid for Scientific Research on Innovative Areas "Neural Diversity and Neocortical Organization" (grant number 22123010); the Strategic Research Program for Brain Sciences "Bioinformatics for Brain Sciences" from the Ministry of Education, Culture, Sports,

Science and Technology (MEXT); the Brain/MIND project from the Japan Agency for Medical Research and Development (AMED); and CREST, JST.

Received: October 22, 2014
Revised: September 6, 2015
Accepted: November 22, 2015
Published: December 24, 2015

REFERENCES

Brenner, S. (1974). The genetics of *Caenorhabditis elegans*. Genetics *77*, 71–94.

Christensen, M., Estevez, A., Yin, X., Fox, R., Morrison, R., McDonnell, M., Gleason, C., Miller, D.M., 3rd, and Strange, K. (2002). A primary culture system for functional analysis of *C. elegans* neurons and muscle cells. Neuron *33*, 503–514.

Clark, D.A., Biron, D., Sengupta, P., and Samuel, A.D. (2006). The AFD sensory neurons encode multiple functions underlying thermotactic behavior in *Caenorhabditis elegans*. J. Neurosci. *26*, 7444–7451.

Dinstein, I., Heeger, D.J., and Behrmann, M. (2015). Neural variability: friend or foe? Trends Cogn. Sci. *19*, 322–328.

Eto, K., Takahashi, N., Kimura, Y., Masuho, Y., Arai, K., Muramatsu, M.A., and Tokumitsu, H. (1999). Ca(2+)/Calmodulin-dependent protein kinase cascade in *Caenorhabditis elegans*. Implication in transcriptional activation. J. Biol. Chem. *274*, 22556–22562.

Han, M., Golden, A., Han, Y., and Sternberg, P.W. (1993). *C. elegans lin-45* raf gene participates in *let-60* ras-stimulated vulval differentiation. Nature *363*, 133–140.

Hashimoto, S., Boissel, S., Zarhrate, M., Rio, M., Munnich, A., Egly, J.-M., and Colleaux, L. (2011). MED23 mutation links intellectual disability to dysregulation of immediate early gene expression. Science *333*, 1161–1163.

Hedgecock, E.M., and Russell, R.L. (1975). Normal and mutant thermotaxis in the nematode Caenorhabditis elegans. Proc. Natl. Acad. Sci. USA *72*, 4061–4065.

Hobert, O., Mori, I., Yamashita, Y., Honda, H., Ohshima, Y., Liu, Y., and Ruvkun, G. (1997). Regulation of interneuron function in the *C. elegans* thermoregulatory pathway by the *ttx-3* LIM homeobox gene. Neuron *19*, 345–357.

Inada, H., Ito, H., Satterlee, J., Sengupta, P., Matsumoto, K., and Mori, I. (2006). Identification of guanylyl cyclases that function in thermosensory neurons of *Caenorhabditis elegans*. Genetics *172*, 2239–2252.

Ito, H., Inada, H., and Mori, I. (2006). Quantitative analysis of thermotaxis in the nematode *Caenorhabditis elegans*. J. Neurosci. Methods *154*, 45–52.

Jurado, P., Kodama, E., Tanizawa, Y., and Mori, I. (2010). Distinct thermal migration behaviors in response to different thermal gradients in *Caenorhabditis elegans*. Genes Brain Behav. *9*, 120–127.

Kandel, E.R., Dudai, Y., and Mayford, M.R. (2014). The molecular and systems biology of memory. Cell *157*, 163–186.

Kim, E., Sun, L., Gabel, C.V., and Fang-Yen, C. (2013). Long-term imaging of *Caenorhabditis elegans* using nanoparticle-mediated immobilization. PLoS ONE *8*, e53419.

Kimura, K.D., Miyawaki, A., Matsumoto, K., and Mori, I. (2004). The *C. elegans* thermosensory neuron AFD responds to warming. Curr. Biol. *14*, 1291–1295.

Komatsu, H., Mori, I., Rhee, J.S., Akaike, N., and Ohshima, Y. (1996). Mutations in a cyclic nucleotide-gated channel lead to abnormal thermosensation and chemosensation in *C. elegans*. Neuron *17*, 707–718.

Kuhara, A., Okumura, M., Kimata, T., Tanizawa, Y., Takano, R., Kimura, K.D., Inada, H., Matsumoto, K., and Mori, I. (2008). Temperature sensing by an olfactory neuron in a circuit controlling behavior of *C. elegans*. Science *320*, 803–807.

Kunitomo, H., Sato, H., Iwata, R., Satoh, Y., Ohno, H., Yamada, K., and Iino, Y. (2013). Concentration memory-dependent synaptic plasticity of a taste circuit regulates salt concentration chemotaxis in *Caenorhabditis elegans*. Nat. Commun. *4*, 2210.

Lisman, J., Schulman, H., and Cline, H. (2002). The molecular basis of CaMKII function in synaptic and behavioural memory. Nat. Rev. Neurosci. *3*, 175–190.

Mori, I., and Ohshima, Y. (1995). Neural regulation of thermotaxis in *Caenorhabditis elegans*. Nature *376*, 344–348.

Nishida, Y., Sugi, T., Nonomura, M., and Mori, I. (2011). Identification of the AFD neuron as the site of action of the CREB protein in *Caenorhabditis elegans* thermotaxis. EMBO Rep. *12*, 855–862.

Ramón y Cajal, S. (1894). The Croonian Lecture: La fine structure des centres nerveux [The fine structure of nerve centers]. Proc. R. Soc. Lond. *55*, 444–468.

Reiner, D.J., Newton, E.M., Tian, H., and Thomas, J.H. (1999). Diverse behavioural defects caused by mutations in *Caenorhabditis elegans unc-43* CaM kinase II. Nature *402*, 199–203.

Sasakura, H., and Mori, I. (2013). Behavioral plasticity, learning, and memory in *C. elegans*. Curr. Opin. Neurobiol. *23*, 92–99.

Satterlee, J.S., Sasakura, H., Kuhara, A., Berkeley, M., Mori, I., and Sengupta, P. (2001). Specification of thermosensory neuron fate in *C. elegans* requires *ttx-1*, a homolog of otd/Otx. Neuron *31*, 943–956.

Satterlee, J.S., Ryu, W.S., and Sengupta, P. (2004). The CMK-1 CaMKI and the TAX-4 Cyclic nucleotide-gated channel regulate thermosensory neuron gene expression and function in *C. elegans*. Curr. Biol. *14*, 62–68.

Sidiropoulou, K., Lu, F.-M., Fowler, M.A., Xiao, R., Phillips, C., Ozkan, E.D., Zhu, M.X., White, F.J., and Cooper, D.C. (2009). Dopamine modulates an mGluR5-mediated depolarization underlying prefrontal persistent activity. Nat. Neurosci. *12*, 190–199.

Singh, N., and Han, M. (1995). *sur-2*, a novel gene, functions late in the *let-60* ras-mediated signaling pathway during *Caenorhabditis elegans* vulval induction. Genes Dev. *9*, 2251–2265.

Tian, L., Hires, S.A., Mao, T., Huber, D., Chiappe, M.E., Chalasani, S.H., Petreanu, L., Akerboom, J., McKinney, S.A., Schreiter, E.R., et al. (2009). Imaging neural activity in worms, flies and mice with improved GCaMP calcium indicators. Nat. Methods *6*, 875–881.

Wayman, G.A., Lee, Y.S., Tokumitsu, H., Silva, A.J., and Soderling, T.R. (2008). Calmodulin-kinases: modulators of neuronal development and plasticity. Neuron *59*, 914–931.

White, J.G., Southgate, E., Thomson, J.N., and Brenner, S. (1986). The structure of the nervous system of the nematode *Caenorhabditis elegans*. Philos. Trans. R. Soc. Lond. B Biol. Sci. *314*, 1–340.

Yu, Y.V., Bell, H.W., Glauser, D.A., Van Hooser, S.D., Goodman, M.B., and Sengupta, P. (2014). CaMKI-dependent regulation of sensory gene expression mediates experience-dependent plasticity in the operating range of a thermosensory neuron. Neuron *84*, 919–926.

Zhang, W., and Linden, D.J. (2003). The other side of the engram: experience-driven changes in neuronal intrinsic excitability. Nat. Rev. Neurosci. *4*, 885–900.

Cell Reports

Supplemental Information

Single-Cell Memory Regulates a Neural Circuit for Sensory Behavior

Kyogo Kobayashi, Shunji Nakano, Mutsuki Amano, Daisuke Tsuboi, Tomoki Nishioka, Shingo Ikeda, Genta Yokoyama, Kozo Kaibuchi, and Ikue Mori

Figure S1

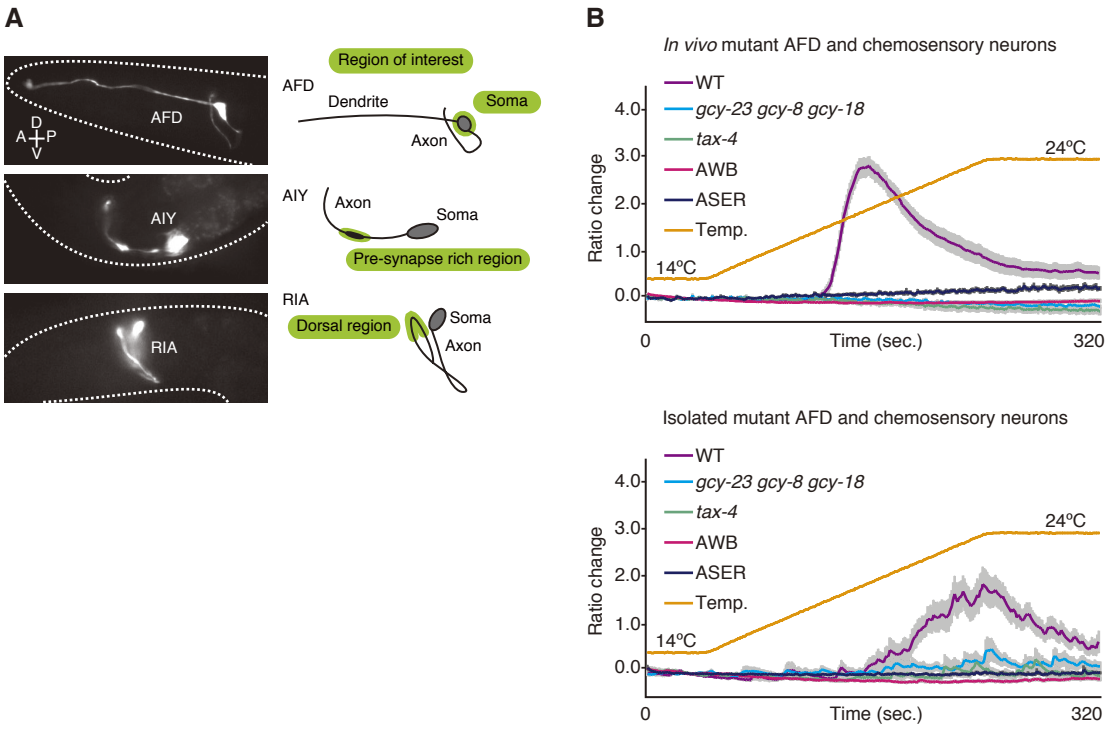
A
AFD
AIY
RIA
D
A
P
V
Region of interest
AFD
Dendrite
Soma
Axon
AIY
Axon
Soma
Pre-synapse rich region
RIA
Dorsal region
Soma
Axon
B
In vivo mutant AFD and chemosensory neurons
WT
gcy-23 gcy-8 gcy-18
tax-4
AWB
ASER
Temp.
24ºC
14ºC
Ratio change
4.0
3.0
2.0
1.0
0.0
0
Time (sec.)
320
Isolated mutant AFD and chemosensory neurons
WT
gcy-23 gcy-8 gcy-18
tax-4
AWB
ASER
Temp.
24ºC
14ºC
Ratio change
4.0
3.0
2.0
1.0
0.0
0
Time (sec.)
320

Figure S1. Calcium imaging of mutant AFD neurons and chemosensory neurons, Related to Figure 1
(**A**) Region of interests in calcium imaging. We quantified fluorescence signals from the soma in AFD, the pre-synapse rich region in AIY axons, and the dorsal region in RIA axons. The pre-synapse rich region in AIY, where the majority of AIY pre-synapses to RIA and AIZ are present (White et al., 1986), and the dorsal region in RIA axons, where most of the pre- and post-synapses to downstream head motor neurons are present (White et al., 1986), showed remarkable changes of intracellular calcium level when subjected to temperature stimuli.
(**B**) Calcium imaging of mutant AFD neurons and chemosensory neurons in *in vivo* (top) or an isolated state (bottom). Wild-type AFD (n = 25 for each in *in vivo* and an isolated state), *gcy-23 gcy-8 gcy-18* mutant AFD (n = 10 in *in vivo* and 34 in an isolated state), *tax-4* mutant AFD (n = 10 in *in vivo* and 22 in an isolated state), olfactory neuron AWB (n = 20 in *in vivo* and 27 in an isolated state) and gustatory neuron ASER (n = 10 in *in vivo* and 36 in an isolated state) cultured at 20 ºC. The purple, blue, green, red and navy lines represent mean ± SEM of ratio change. The orange line indicates temperature.

Figure S2

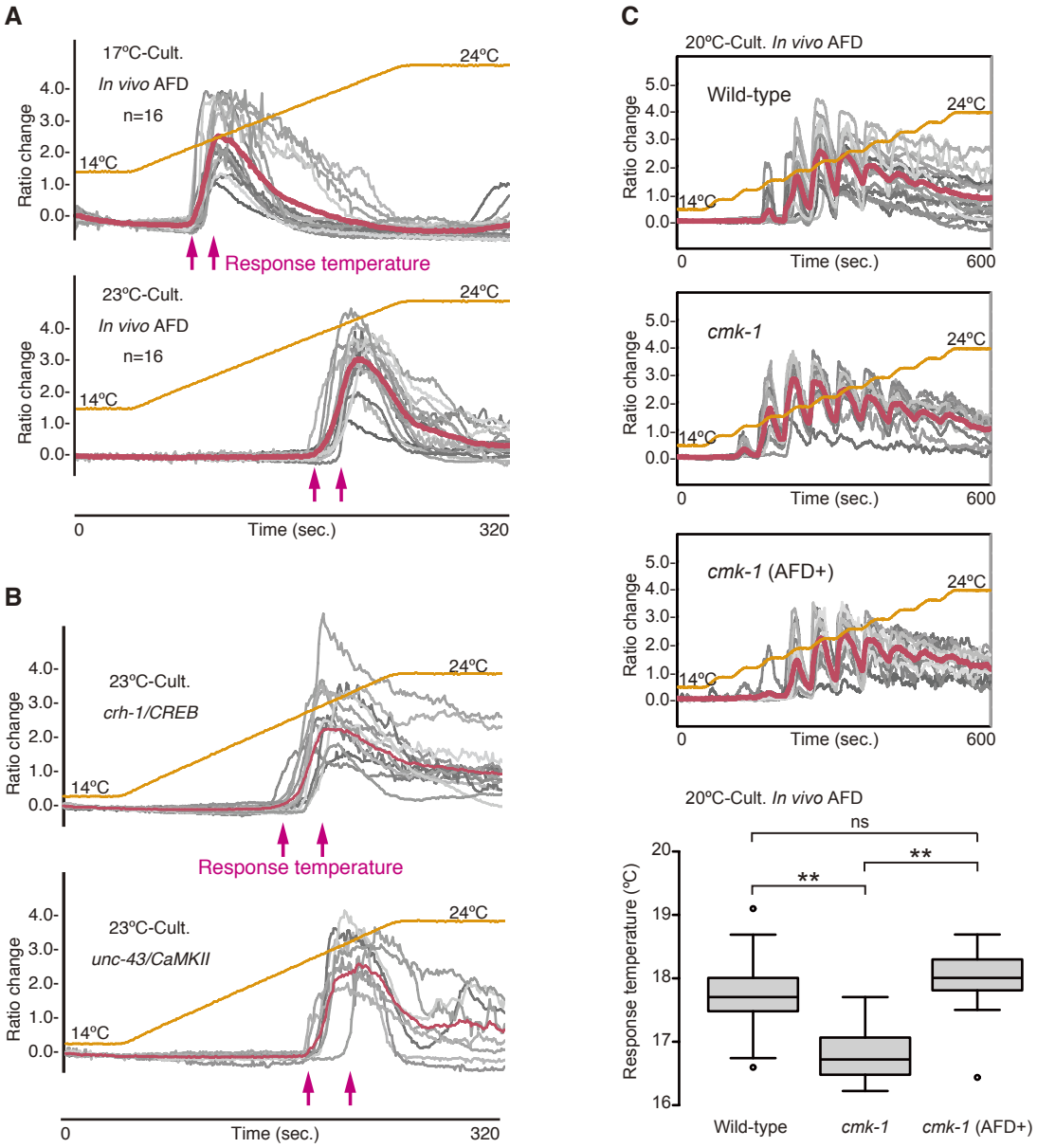
A
17ºC-Cult.
In vivo AFD
n=16
24ºC
14ºC
Ratio change
Response temperature
23ºC-Cult.
In vivo AFD
n=16
Time (sec.)
0
320
B
23ºC-Cult.
crh-1/CREB
Response temperature
23ºC-Cult.
unc-43/CaMKII
C
20ºC-Cult. In vivo AFD
Wild-type
cmk-1
cmk-1 (AFD+)
Time (sec.)
600
Response temperature (ºC)
ns
**
Wild-type
cmk-1
cmk-1 (AFD+)

Figure S2. Calcium imaging of *in vivo* AFD neurons, Related to Figure 2

(**A**) Single-trial calcium imaging of *in vivo* AFD neurons cultivated at 17 ºC (top) or 23 ºC (bottom) (n = 16 for each). The gray lines indicate individual traces of ratio change, and the red line represents the average of individual ratio changes. The orange line indicates temperature. The red arrows indicate the lowest and highest response temperatures.

(**B**) Calcium imaging of AFD in *crh-1*/*CREB* mutants (n = 13) and *unc-43/CaMKII* mutants (n = 8). The gray lines indicate individual traces of ratio change, and the red lines represent the average of individual ratio changes. The orange line indicates temperature. The red arrows indicate the lowest and highest response temperatures.

(**C**) Calcium imaging of AFD in wild-type animals (n = 17), *cmk-1* mutants (n = 12) and *cmk-1* mutants expressing a wild-type *cmk-1* cDNA only in AFD (n = 15) cultivated at 20 ºC. The gray lines indicate individual traces of ratio change, and the red lines represent the average of ratio changes. The orange line indicates temperature. The box plot represents response temperatures.

Figure S3

A

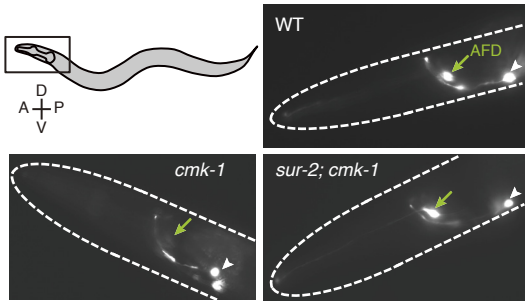

B

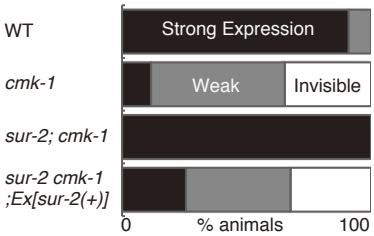

C

Candidate substrates for CaMK1 determined by phosphoproteomic analysis

Candidate substrates
ABCF-3, C46G7.2, F42G9.1, HPO-34, IFFB-1, IMA-3, ITX-1, KETN-1, LIN-45, LPIN-1, MEL-32, MVK-1, MYO-3, NRA-1, PCK-2, PFK-1, PKC-1, PKC-2, RET-1, RLA-1, RPL-23, RPL-24.1, RPS-2, RPS-9, RSP-1, RSP-8, T23E7.2, TFG-1, TIAR-3, TPS-1, UNC-15, UNC-22, UNC-89, VAB-10, VIG-1, WARS-1, Y71F9AL.9, ZYG-9

D

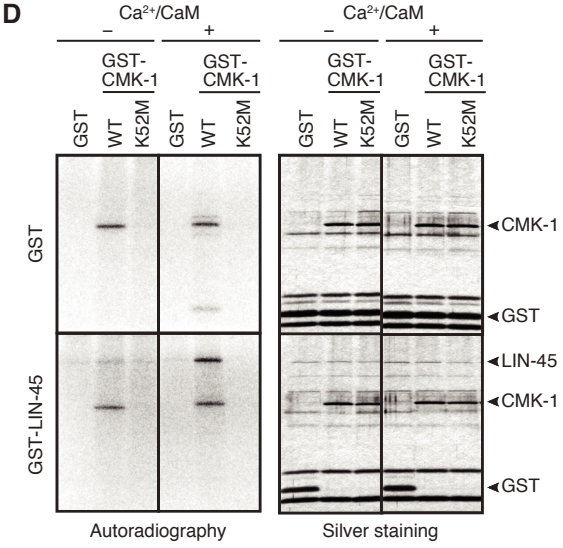

Figure S3. LIN-45 is a downstream target of CMK-1, Related to Figure 3

(**A**) Expression of *nhr-38* promoter-fused GFP (*nhr-38p::GFP*), an AFD specific GFP reporter, and AIY promoter-fused GFP (*AIYp::GFP*), an AIY neuron specific GFP marker, in wild-type animals, *cmk-1* mutants and *sur-2; cmk-1* double mutants. The arrows indicate AFD soma and the arrowheads AIY soma.

(**B**) Percentage of animals with strong (black), weak (gray) or no expression (white) of *nhr-38p::GFP* in wild-type animals (n = 206), *cmk-1* mutants (n = 205), *sur-2; cmk-1* double mutants (n = 205) and *sur-2; cmk-1* double mutants expressing genomic *sur-2* gene (n = 93) cultivated at 25 ºC.

(**C**) Candidate substrates for CaMK1 determined by phosphoproteomic analysis. *C. elegans* were homogenized in lysis buffer (50 mM HEPES at PH7.6, 1 mM DTT, 1 mM EGTA, 50 mM NaCl, 1 mM $MgCl_2$, 0.22 M Sucrose, 10 μM pepstatin, protease inhibitor cocktail (F.Hoffmann-La Roche Ltd, Basel, Schweiz)) by sonication, and centrifuged at 100,000g for 30 minutes. The supernatant were precleared with Glutathione-Sepharose 4B (GE Healthcare UK Ltd., England). Recombinant GST-CaMK1delta (NP_065130.1, 1-357aa, Carna Biosciences, Japan) and GST-CaMK1alpha (NP_604463.1, 1-290aa) prepared in a baculovirus expression system were immobilized on Glutathione-Sepharose 4B, and incubated with *C. elegans* lysate. After washing, the bound proteins with kinase were incubated with (for phosphorylated sample) or without ATP/Mg^{2+} (for nonphosphorylated sample). The proteins including kinase and interactors were subjected to LC/MS/MS analyses as described previously (Amano et al., 2015). A peak list was generated and calibrated using MaxQuant software (version1.2.2.5) (Cox and Mann, 2008). Database searches were performed against the complete proteome set of *Caenorhabditis elegans* in UniProtKB 2012_02 concatenated with reversed copies of all sequences (Peng et al., 2003). The ion intensities of the identified peptides in the phosphorylated sample were compared with those of the nonphosphorylated sample. The proteins containing phosphorylated peptides exhibiting greater than fivefold higher ion intensity were regarded as candidate substrates independently of Phospho (STY) Probability scores. Phosphorylation site localization required a Phospho (STY) Probability score >0.75.

(**D**) Autoradiography (left) and silver staining (right) of *in vitro* phosphorylation assay. GST (top panels) or GST-LIN-45 (bottom panels) were incubated with GST, GST-CMK-1(wild-type) or GST-CMK-1(K52M) in the presence or absence of Ca^{2+}/Calmodulin. pEF-BOS-GST-LIN-45 and pEF-BOS-GST-CMK-1 or pEF-BOS-GST-CMK-1-K52M were cotransfected into COS7 cells, and pulled down with Glutathione-Sepharose 4B. The precipitates were incubated in 50 μl of kinase reaction mixture (25 mM Tris/HCl at pH 7.5, 1 mM EDTA, 1 mM EGTA, 1 mM DTT, 5 mM $MgCl_2$, 2 mM $CaCl_2$, 0.2 mM Calmodulin, 50 μM [γ-^{32}P] ATP [1 to 20 GBq/mmol]) for 30 minutes at 30˚C. The reaction mixtures were boiled in SDS sample buffer and subjected to SDS-PAGE. The radiolabeled proteins were analyzed by an image analyzer (FLA9000; GE Healthcare). This experiment was successfully reproduced multiple times.

Figure S4

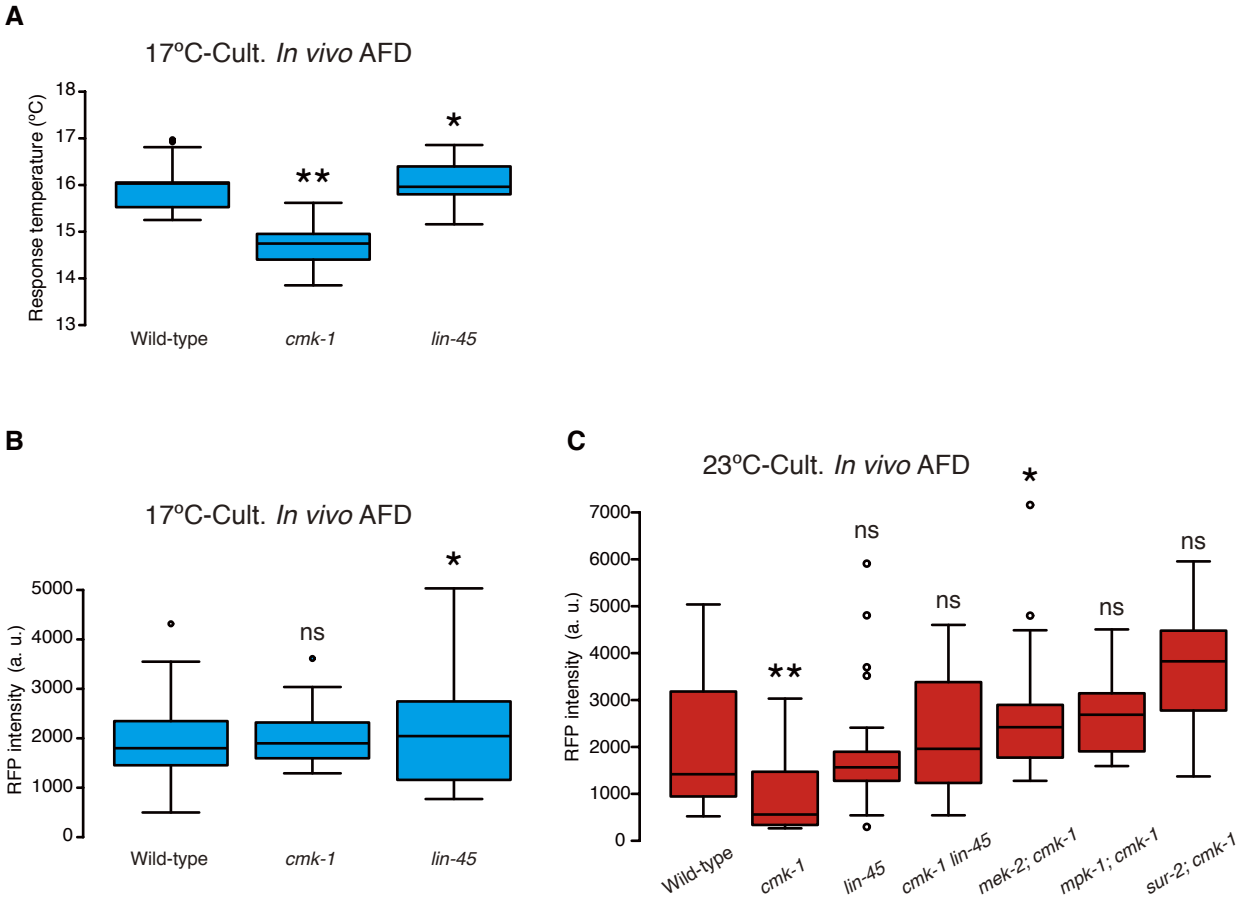
A
17ºC-Cult. *In vivo* AFD
Response temperature (ºC)
18
17
16
15
14
13
**
*
Wild-type
cmk-1
lin-45
B
17ºC-Cult. *In vivo* AFD
RFP intensity (a. u.)
5000
4000
3000
2000
1000
0
ns
*
Wild-type
cmk-1
lin-45
C
23ºC-Cult. *In vivo* AFD
RFP intensity (a. u.)
7000
6000
5000
4000
3000
2000
1000
0
**
ns
ns
*
ns
ns
Wild-type
cmk-1
lin-45
cmk-1 lin-45
mek-2; cmk-1
mpk-1; cmk-1
sur-2; cmk-1

Figure S4. Expression level of *gcy-8* gene, Related to Figure 3

(**A**) Box plot of response temperatures. Wild-type animals (n = 17), *cmk-1* mutants (n = 15) and *lin-45* mutants (n = 13) cultivated at 17 ºC were subjected to stepwise temperature warming. Steel test was applied to compare the response temperatures in mutants with that in wild-type controls.

(**B** and **C**) Box plot of RFP fluorescence intensities. RFP intensities of AFD from *njIs24[gcy-8p::TagRFP, gcy-8p::GCaMP3]* integrated transgene were calculated from the calcium imaging data shown in Figure S4A (B) and Figure 3 (C). The average values of RFP intensities of the first 50 seconds before the initiation of temperature warming were used for the box plots. Steel test was applied to compare the RFP intensities in mutants with that in wild-type controls.

Table S1. Number of samples that exceeded 1.0 GCaMP3/TagRFP fluorescence ratio change, Related to Figure 1

		(Number of samples that exceeded 1.0 ratio change) / (Total Number of samples) (%)	
Neuron	**Genotype**	***In vivo* (20 ºC-Cult.)**	**Isolated (20 ºC-Cult.)**
AFD	Wild-type	58/61 (95.1 %) shown in Fig. 1E	38/45 (84.4 %) shown in Fig. 1F
	Wild-type	24/25 (96.0 %) shown in Fig. S1B	24/25 (96.0 %) shown in Fig. S1B
	gcy-23 gcy-8 gcy-18	0/10 (0 %) shown in Fig. S1B	17/34 (50.0 %) shown in Fig. S1B
	tax-4	0/10 (0 %) shown in Fig. S1B	7/22 (31.8 %) shown in Fig. S1B
AWB	Wild-type	0/20 (0 %) shown in Fig. S1B	2/27 (7.4 %) shown in Fig. S1B
ASER	Wild-type	0/10 (0 %) shown in Fig. S1B	2/36 (5.6 %) shown in Fig. S1B

Table S2. Strains used in this study, Related to Experimental Procedures

Strain name	Genotype
Bristol N2	Wild-type
IK1296	*njEx567[ttx-1p::GFP, gcy-8-TagRFP]*
IK0961	*njIs24[gcy-8p::GCaMP3, gcy-8p::TagRFP] (I)*
IK0980	*njIs24; gcy-23(nj37) gcy-8(oy44) gcy-18(nj38)*
IK1154	*njIs24; tax-4(p678)*
IK0860	*njEx618[gcy-5p::GCaMP3, gcy-5p::TagRFP]*
IK0859	*njEx476[str-1p::GCaMP3, str-1p::TagRFP]*
IK0972	*njIs24; crh-1(tz2)*
IK1286	*njIs24; unc-43(n1186)*
PY1589	*cmk-1(oy21)*
IK1033	*cmk-1(oy21); njEx414[ttx-1p::cmk-1cDNA(+), ges-1p::nls-GFP]*
IK2030	*cmk-1(oy21); njEx745[ttx-1p::cmk-1cDNA(K52M), ges-1p::nls-GFP]*
IK1013	*njIs24; cmk-1(oy21)*
IK1129	*njIs24; cmk-1(oy21); njEx414*
IK1764	*njIs24; lin-45(dx84)/nT1[qIs51]; +/nT1[qIs51]*
IK1857	*njIs24; cmk-1(oy21) lin-45(dx84)/cmk-1(oy21) nT1[qIs51]; +/nT1[qIs51]*
IK1911	*njIs24; cmk-1(oy21) lin-45(dx84)/cmk-1(oy21) nT1[qIs51]; +/nT1[qIs51]; njEx692[ttx-1p::lin-45(+)cDNA, ges-1p::nls-GFP]*
IK1776	*mek-2(n2678)/hT2[qIs48]; +/hT2[qIs48]; njEx359[gcy-8p::GCaMP3, gcy-8p::TagRFP]*
IK1700	*mek-2(n2678)/hT2[qIs48]; +/hT2[qIs48]; cmk-1(oy21); njEx359*
IK1805	*njIs24; mpk-1(ga117)/qC1[nIs189]*
IK1807	*njIs24; mpk-1(ga117)/qC1[nIs189]; cmk-1(oy21)*
IK1355	*njIs24 sur-2(nj73)*
IK1357	*njIs24 sur-2(nj73); cmk-1(oy21)*
IK1144	*njIs26[AIYp::GCaMP3, AIYp::TagRFP, ges-1p::nls-TagRFP] (X)*
IK1289	*gcy-23(nj37) gcy-8(oy44) gcy-18(nj38); njIs26*
IK1404	*njIs30[glr-3p::GCaMP3, glr-3p::TagRFP, ges-1p::nls-TagRFP] (V)*
IK1425	*gcy-23(nj37) gcy-8(oy44) gcy-18(nj38); njIs30*
IK1565	*njIs30; ttx-3(ks5)*
IK0673	*njIs2[nhr-38p::GFP, AIYp::GFP] (V)*
IK0778	*cmk-1(oy21); njIs2*

IK0788	*sur-2(nj73); cmk-1(oy21); njIs2*
IK0858	*sur-2(nj73); cmk-1(oy21); njIs2; njEx475[genomic sur-2* (+)*, ges-1p::nls-GFP]*
IK1273	*cmk-1(oy21); njIs26*
IK1533	*cmk-1(oy21); njIs26; njEx414*

Supplemental Experimental Procedures

Primary cell culture. We isolated eggs from gravid animals cultivated in S-basal buffer (100 mM NaCl, 25 mM KPO_4 pH 6.0, 5 mg/L cholesterol) with *E. coli* OP50 as a food source and spread dissociated embryonic cells at a low cell density (~9 x 10^4 cells / cm^2) onto 5 mm square microscope cover glass (Matsunami Glass Ind. Ltd., Japan) coated with peanut lectin. The cell-seeded cover glasses were left on the bottom of 35 mm diameter petri dishes with 2 ml of culture medium. Culture medium was frequently exchanged (every day and immediately before fluorescence imaging).

Calcium imaging. Adult animals and two- to three-day old cultured cells expressing cell specific promoter-driven GCaMP3 were used for calcium imaging. For *in vivo* calcium imaging, a single adult animal was placed on a 10 % agar pad on a microscope coverslip with 0.4 µl of 0.1 µm polystyrene beads (Polysciences) and covered by a coverslip to immobilize the animals (Kim et al., 2013). The coverslip, agar pad and beads solution were kept at the initial imaging temperature. For isolated cells, a cell-plated 5 mm square microscope coverslip was washed with extracellular solution (145 mM NaCl, 5 mM KCl, 5 mM $MgCl_2$, 1 mM $CaCl_2$, 10 mM HEPES, 10 mM, D-glucose, pH adjusted with NaOH to 7.2 and osmolality adjusted with sucrose to 340 mOsm) and placed in a square hole (54 mm on each side and 0.2 mm deep) made by cutting Polyethylene Terephthalate that was glued on a 24 mm square coverslip. Then 14 µl of extracellular solution was added to the chamber before covering it with a coverslip. The coverslip and extracellular solution were kept at the initial imaging temperature. Sample preparation of both live animals and cultured cells were completed within 2 minutes. Samples were then placed onto a peltier-based thermocontroller (Tokai Hit, Japan) on the stage of an Olympus BX61WI at the initial imaging temperature for 5 minutes. The fluorescence was separated by a Dual-View (Molecular devices) optics systems and GCaMP3 and TagRFP images were then captured by an EM-CCD camera C9100-13 ImagEM (Hamamatsu Photonics, Japan). Using a pulse generator SG-4115 (IWATSU, Japan), images were taken with a 100 ms excitation pulse at a 1 Hz frame rate with 1 x 1 binning. The temperature on the agar pad was monitored by a thermometer system, DCM-20 (Tokai Hit and Hamamatsu Photonics). For each imaging experiment, fluorescence intensities were measured using the MetaMorph (Molecular Device) imaging analysis system.

Calculations of trial-to-trial variability and animal-to-animal variability. Trial-to-trial variability was calculated as the following formula:

$$\frac{1}{N-1}\sum_{j=2}^{N}\left|x_{jm}-x_{(j-1)m}\right|,$$

where x_{jm} = response temperature recorded in the j-th trial of the animal m, m = {1, 2, 3, ... , M (M = 19 for wild-type animals and 8 for *cmk-1* mutants and isolated cells)} and N = total number of trials per animal (in this study, N = 6). Animal-to-animal variability was calculated as the following formula:

$$\frac{1}{N}\sum_{j=1}^{N}\left\{Max(\mathbf{y}_j)-Min(\mathbf{y}_j)\right\},$$

where $\mathbf{y}_j=\left\{x_{j1},x_{j2},x_{j3},\cdots,x_{jM}\right\}$.

Supplemental Results

The CaMKI/IV and Raf pathway regulates the *gcy-8* gene expression

Since our analysis showed that the output of the Raf pathway in AFD is through SUR-2, a transcriptional regulator, we asked if the variability in AFD responses could be attributed to the regulation of gene expression in AFD. A previous study suggested that CMK-1 promotes the expression of an AFD specific guanylyl cyclase GCY-8 and other thermosensory transduction molecules, thereby mediating the operating range of the AFD thermal response (Yanxun et al., 2014). We then analyzed both the expression level of *gcy-8* and response temperature, and found that AFD neurons of 17 ºC-cultivated *cmk-1* mutants showed abnormality in neither the *gcy-8* expression nor the variability in response temperature, although the operating range of AFD was abnormally low (Figures S4A and S4B). By contrast, AFD neurons of 23 ºC-cultivated *cmk-1* mutants showed decreased expression of *gcy-8* and increased variability of AFD responses (Figures 3D and S4C). Since both of these *cmk-1* abnormalities were restored to the wild-type phenotype in the Raf pathway mutant background (Figures 3D and S4), the increased variability of AFD could result from the decreased expression of *gcy-8*. Thus, these results suggest that the CaMKI/IV and Raf pathway-mediated gene expression likely contributes to the individual differences in AFD single-cell memory.

Supplemental References

Amano, M., Hamaguchi, T., Shohag, M.H., Kozawa, K., Kato, K., Zhang, X., Yura, Y., Matsuura, Y., Kataoka, C., Nishioka, T.*, et al.* (2015). Kinase-interacting substrate screening is a novel method to identify kinase substrates. J Cell Biol *209*, 895-912.

Cox, J., and Mann, M. (2008). MaxQuant enables high peptide identification rates, individualized ppb-range mass accuracies and proteome-wide protein quantification. Nature biotechnology *26*, 1367-1372.

Peng, J., Elias, J.E., Thoreen, C.C., Licklider, L.J., and Gygi, S.P. (2003). Evaluation of multidimensional chromatography coupled with tandem mass spectrometry (LC/LC-MS/MS) for large-scale protein analysis: the yeast proteome. Journal of proteome research *2*, 43-50.